The Astrophysical Journal, 793:54 (7pp), 2014 September 20 doi:10.1088/0004-637X/793/1/54

THE DYNAMIC CHARACTER OF THE POLAR SOLAR WIND

B. V. Jackson, H.-S. Yu, A. Buffington, and P. P. Hick
Center for Astrophysics and Space Sciences, University of California, San Diego, La Jolla, CA 92093-0424, USA;
bvjackson@ucsd.edu, hsyu@ucsd.edu, abuffington@ucsd.edu, pphick@ucsd.edu
Received 2014 April 11; accepted 2014 July 21; published 2014 September 5

ABSTRACT

The *Solar and Heliospheric Observatory* (*SOHO*) Large Angle and Spectrometric Coronagraph C2 and *Solar Terrestrial Relations Observatory* (*STEREO*) COR2A coronagraph images, when analyzed using correlation tracking techniques, show a surprising result in places ordinarily thought of as "quiet" solar wind above the poles in coronal hole regions. Instead of the static well-ordered flow and gradual acceleration normally expected, coronagraph images show outflow in polar coronal holes consisting of a mixture of intermittent slow and fast patches of material. We compare measurements of this highly variable solar wind from C2 and COR2A images and show that both coronagraphs measure essentially the same structures. Measurements of the mean velocity as a function of height of these structures are compared with mass flux determinations of the solar wind outflow in the large polar coronal hole regions and give similar results.

Key words: solar wind – Sun: corona – Sun: heliosphere

Online-only material: animations, color figures

1. INTRODUCTION

In situ observations from the *Ulysses* spacecraft (McComas et al. 1998a) have shown that the polar solar wind appears relatively uniform with little change in velocity (Phillips et al. 1994) at 2 AU during solar minimum, when large polar coronal holes are the main contributors to high-speed solar wind in these regions (McComas et al. 1998b, 2008). At these times, coronagraph observations, on average, show depressed brightness, implying low-density and high-speed wind emanates from the coronal holes. The solar wind momentum flux (mv^2) is nearly constant at *Ulysses* distances from the Sun whether or not there is a coronal hole and a low-density origin for the solar wind (Phillips et al. 1995).

However, near the solar surface, polar coronal hole regions are anything but "quiet" and show highly dynamic chromospheric and coronal phenomena, such as spicules, macrospicules, and X-ray jets (e.g., Shibata 1982; Wang et al. 1998a). Furthermore, observations of comet plasma tail changes by spaceborne heliospheric imagers (Buffington et al. 2008; Clover et al. 2010; Jackson et al. 2013) show that coronal solar wind speeds between the solar surface and 1 AU in polar regions are highly variable. The characteristics of this variability have been studied extensively at 1 AU in the ecliptic using in situ measurements of the magnetic field and plasma (e.g., Borovsky 2008, 2012); see also Feldman et al. (1997) for suggestions that the solar wind may be "pulsed."

Yu et al. (2014) reintroduced a two-dimensional (2D) cross-correlation technique, first termed optical flow by Horn & Schunck (1981), to measure the outward motion of discrete structures associated with solar jets in coronagraph images. Figure 1 shows an example based on images from the *Solar and Heliospheric Observatory* (*SOHO*) Large Angle and Spectrometric Coronagraph (LASCO) C2 (Brueckner et al. 1995). The "speed map" (Figure 1(b)) shows a striking new view of the solar wind in the polar region as a population of patches with high and low solar wind speed existing side by side across the whole region. Areas of high and low speed are elongated more or less radially and change continuously with time. Thus, not only does the solar wind above the largest jets contain high-speed bursts of material, but so does the whole of the corona above polar hole regions; this is a new result. In most coronal observations, the polar coronal hole regions have low density and appear as uniform features; in solar wind as observed by *Ulysses*, the polar hole regions are extremely uniform and non-structured. In the lower corona, the present analysis shows that the variability in bulk outward solar wind motion can be as great as an order of magnitude! With this result, we are able to explain some previously not understood or misunderstood features of solar polar coronal holes.

This article maps the polar high-speed solar wind variability in LASCO C2 and the *Solar Terrestrial Relations Observatory* (*STEREO*) COR2A (Howard et al. 2008) coronagraph images using the above cross-correlation technique. We explore the variable nature of the polar solar wind structures and their general evolution with distances from the Sun. Section 2 describes the methodology and measurements. Section 3 presents the results. Section 4 gives the discussion of our analyses. We summarize our results in Section 5.

2. METHODOLOGY AND MEASUREMENTS

Jackson & Hick (1997a, 1997b) and Jackson et al. (1998) developed a 2D cross-correlation technique to measure coronal outflow in a pair of consecutive coronagraph images by measuring patches of small-scale bright and dark coronal features; this technique was recently modified to provide speed maps of these coronal structures using data from LASCO C2 and *STEREO* COR2A images. This cross-correlation technique has previously been used to determine speeds of the coronal solar jetting response in both these data sets (Figure 1; as in Yu et al. 2013, 2014). A speed is found by selecting an area of sky located in the first (earlier) image (Figure 1(a)), and then by exploring a range of equivalent areas of the later image whose center locations lie within an acceptable outer boundary (as in Figure 1(a)), to find that later image's particular location, whose area has the highest brightness correlation with the first area. Then the 2D "plane of the sky" speed for that first-image location is the distance between the locations of the highest correlation position relative to the center of the first area divided by the time

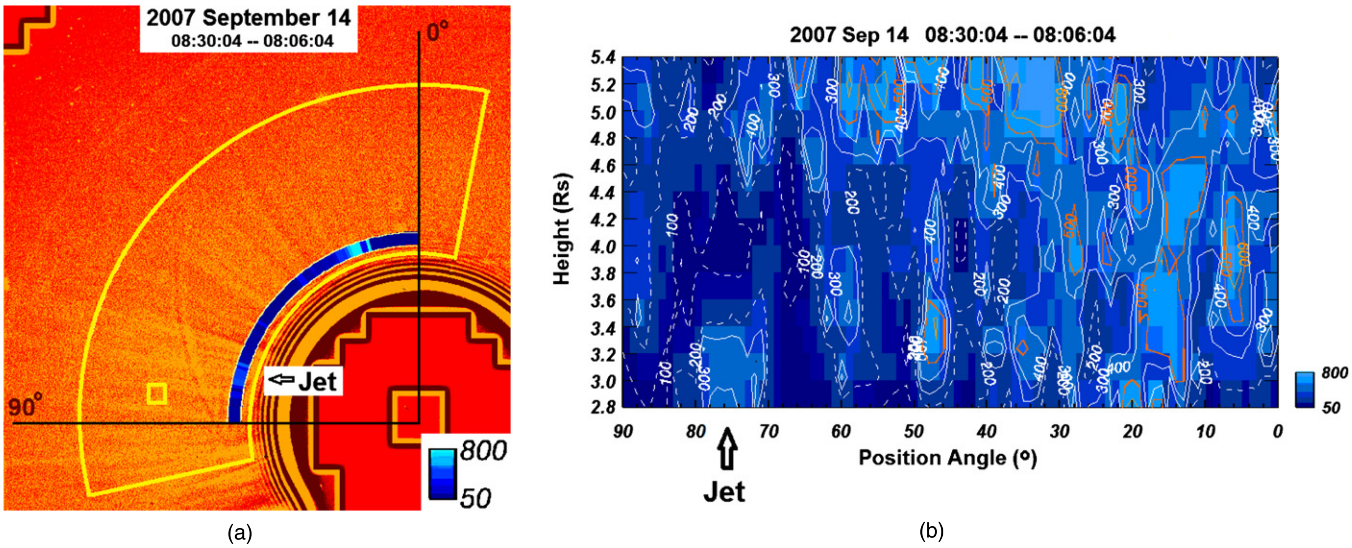

Figure 1. (a) LASCO C2 background subtracted image on 2007 September 14 at 08:06:04 UT, with the speeds at 2.8 R_s from P.A.s of 0° to 90° superposed in blue (marked on the image) obtained from a 2D cross-correlation with a later image at 08:30:04 UT. The small yellow square indicates the size of the correlation area (0.4 R_s × 0.4 R_s); the area bounded by the yellow inner and outer arcs and radials is the region explored here by the correlation technique. The range of speeds shown, from 50 to 800 km s^{-1}, is given in the lower right corner. (b) Map of the solar wind speed at different heights and P.A.s obtained by the correlation technique (see Section 2 for details). The arrow in panels (a) and (b) marks the response of a large jet, moving outward at a speed of over 400 km s^{-1} into a region of slower flow. This response speed was confirmed by direct inspection of coronagraph difference images.

(A color version of this figure is available in the online journal.)

difference between the two images. We proceed by covering a given region of interest in the first image with a regular grid of solar elongation distances in solar radii (R_s) and position angles (P.A.s, or angular distance measured counterclockwise from the north heliographic pole). We then apply the above method using an area centered at each of these grid locations, find its corresponding speed, and construct a map having this speed at each of the grid's various locations (Figure 1(b)).

Several different grid increments and correlation areas were explored. The COR2A image resolution (15 arcsec pixel^{-1}) is roughly the same as C2 (12 arcsec pixel^{-1}). Radial increments chosen for C2 and COR2 were 0.2 R_s and 0.4 R_s, respectively, and 1° in P.A. for both. The location of the correlation was further restricted to lie within an off-radial angle of 20° from the particular grid location of the first image. We experimented with different-sized correlation areas for the images (the yellow square in Figure 1(a)) and settled on a size of 31 × 31 pixels (∼0.4 R_s); changing this characteristic size did not significantly alter the results obtained. Once these resolutions, angular limits, and correlation areas were chosen, they remained fixed in the subsequent analyses.

Figure 2 shows the speed map resulting from cross-correlating image pairs from COR2A and from C2. A similar corresponding "brightness map" is produced by assigning the brightness of the high-correlation location in the later image to the location of the area in the early image. An example of such a brightness map is shown in Figure 3.

For all these analyses, the coronagraph images were pre-processed by subtracting the average of all available coronagraph images over about 6 to 8 hr, a time much longer than the 24 minute image cadence for C2 and the 30 minute cadence for COR2A. Furthermore, the images, 1024 × 1024 pixels for C2 and 2048 × 2048 pixels for COR2A, were smoothed by averaging over 9 × 9 pixels generating a smoothed area of ∼0.1 R_s in height and from 0°.5 to a few degrees in P.A. depending on the distance from the Sun. To provide consistent results independent of the choice of lower and upper bounds on the allowed speeds,

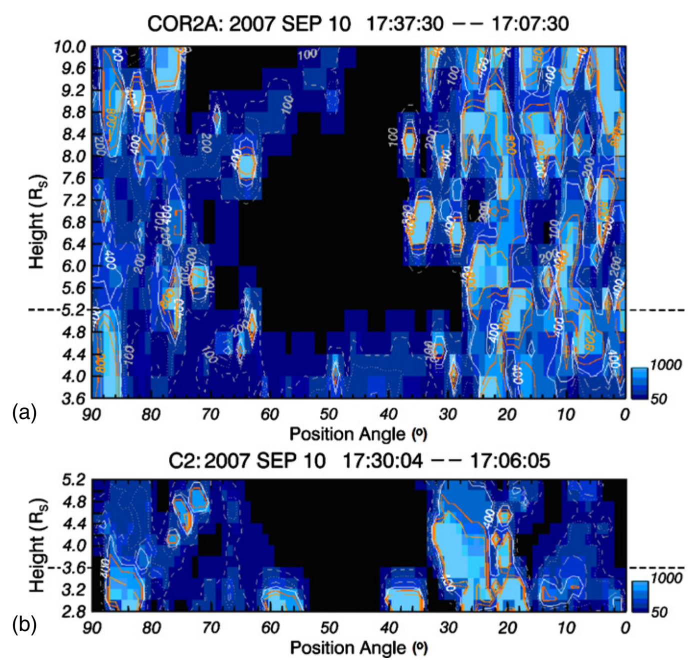

Figure 2. Speed maps derived from COR2A and C2 image pairs on 2007 September 10. (a) From COR2A images at 17:07:30 UT and 17:37:30 UT, extending from 3.6 to 10.0 R_s and from 90° east to 0° at the solar north pole. A dashed line at 5.2 R_s on the right and left edge indicates the upper boundary of the C2 map in panel (b). (b) From C2 images at 17:06:05 UT and 17:30:04 UT, extending from 2.8 to 5.2 R_s and covering the same P.A. range as in panel (a). A dashed line at 3.6 R_s on the right and left edge shows the lower boundary of the COR2A map in panel (a).

(Animations and color version of this figure are available in the online journal.)

correlations were required to be greater than 0.5. We allowed speeds ranging from 50 to 1000 km s^{-1}, and also from 50 to 1500 km s^{-1}, and found the locations of lower speed patches virtually the same for both speed ranges. A few additional high-speed patches appear for the larger speed range. We note that

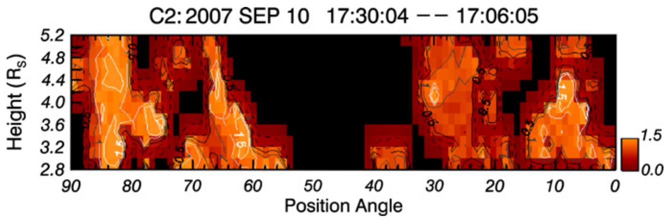

Figure 3. Brightness map determined from the same pair of consecutive LASCO C2 observations as used for the speed map in Figure 2(b).

(A color version of this figure is available in the online journal.)

both a direct and a correlation speed measurement of a polar jet response of over 1300 km s^{-1} was recorded for one feature by Yu et al. (2013). Locations where we find no correlations higher than 0.5 are not assigned a speed and are black in Figures 2 and 3.

In order to substantiate that the dynamic polar speeds measured have the same general structure in images from different coronagraphs, we analyzed different periods for C2 and COR2A near the *STEREO* launch date in 2007. We searched for image pairs from both instruments with approximately the same start times in order to ensure that the same features are seen by both. Additionally, we selected areas in the images covering the regions above the large northern polar coronal hole seen in data from the *Hinode* spacecraft X-Ray Telescope (Golub et al. 2007) and the *SOHO* EUV Imaging Telescope (EIT; Delaboudinière et al. 1995) that were as much as possible free of coronal mass ejections (CMEs). Figure 2(a) shows a speed map for a polar region in COR2A data, and Figure 2(b) shows this same region in C2. We find that COR2A speed maps show an irregular patchwork of high- and low-speed coronal solar wind structures and that the same approximate character is seen in C2 maps. Where the two maps overlap, many of the structures have about the same speed at the same location. The speeds obtained from each $3^\circ \times 0.8\ R_s$ area in the C2 map compared with the corresponding COR2A location in Figure 2 from 20° to 70° in P.A. have a positive correlation of ∼0.41 (Figure 4). Hence, both instruments observe approximately the same high- and low-speed polar coronal features even though the views in 2007 September from C2 and COR2A are 17° apart from one another in ecliptic longitude, and the coronagraph images do not have exactly simultaneous start and end times.

To explore the relationship between speed and brightness above the solar poles, we correlated the brightness (Figure 3) from each 3° by 0.8 R_s area from P.A.s of from +60° to −60° with the speed at those locations. Figure 5 presents the result.

Table 1 lists the data sequences analyzed that have start times within eight minutes of one another in both C2 and COR2A image sets (Columns 2 and 3). We give these speed correlations of the areas in common between C2 and COR2A covering the polar regions from 20° to 70° in P.A. Similar positive correlations for high- and low-speed coronal wind patches are generally present for other simultaneous C2 and COR2A image sequences during the periods we studied, and are presented in Column 4 of Table 1. The results in general are in agreement with those we show as examples in Figures 2 and 4. We also give the correlations of brightness for the 20° to 70° in P.A. areas in common between C2 and COR2A over the polar regions in Column 5 of Table 1, and these again generally give positive correlations. In the studies of observations of speed versus brightness for either C2 or COR2A such as are shown in Figure 5, we also find a positive correlation that persists for each image sequence measured (Columns 6 and 7 of

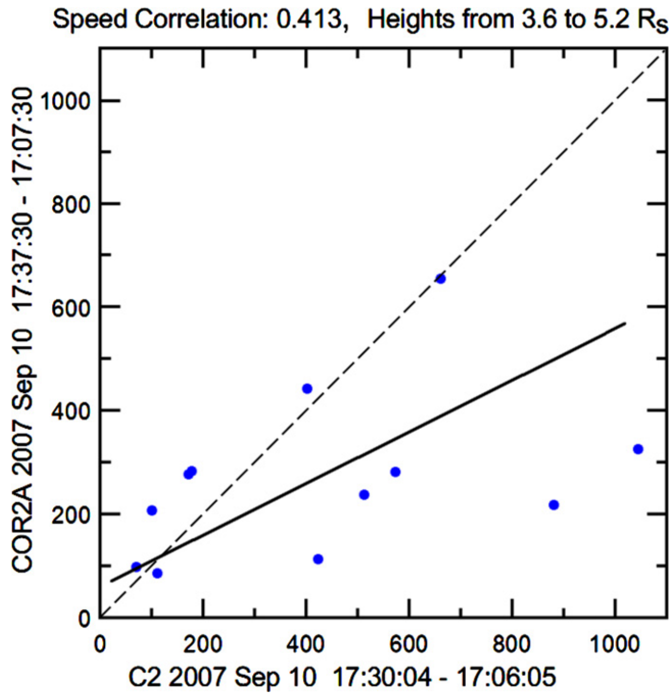

Figure 4. Comparison of the common region of the two speed maps of Figure 2 for P.A.s of 20° to 70° on 2007 September 10. The dashed line shows a one-to-one correspondence between the data sets.

(A color version of this figure is available in the online journal.)

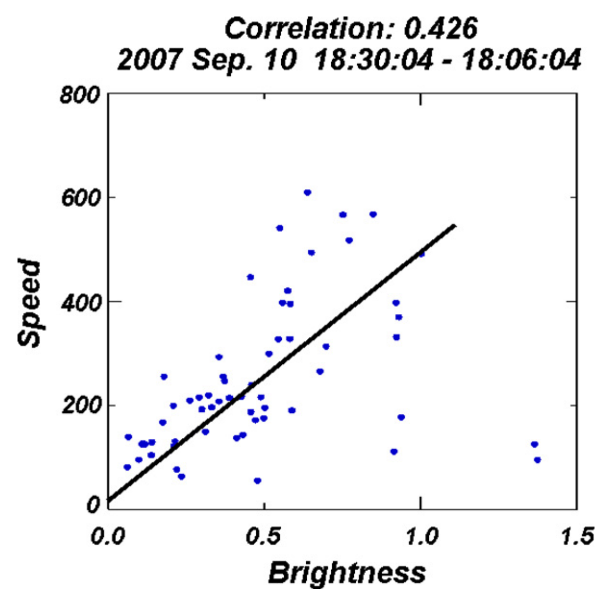

Figure 5. Comparison of the coronal speed in Figure 2(b) with coronal brightness of the C2 image from 3.6 to 5.2 R_s. A positive correlation of speed with coronal brightness is shown in the region from P.A.s of +60° to −60° on 2007 September 10.

(A color version of this figure is available in the online journal.)

Table 1). Thus, we find that the high-speed patches are generally associated with locations of higher brightness patches, similar to the enhancements associated with the jetting onsets measured by Yu et al. (2014).

3. AVERAGE SPEED RESULTS

Figure 6 shows the speed of the coronal structures with a height for C2 (at 3.4 R_s) and COR2A over solar P.A. To obtain

Table 1
Speed and Brightness Correlations from Images with Near-identical Start Times

Date in 2007	C2 Time (UT)	COR2A Time (UT)	C2–COR2A Speed Correlation	C2–COR2A Brightness Correlation	C2 Speed to Brightness Correlation	COR2A Speed to Brightness Correlation
Mar 2	13:24:04–13:12:04	13:42:00–13:12:00	0.345	0.653	0.668	0.225
Mar 3	13:24:04–13:12:06	13:42:00–13:12:00	0.086	0.578	0.646	0.082
Mar 4	13:24:05–13:12:07	13:42:00–13:12:00	...	0.490	0.493	0.166
Sep 10	16:30:05–16:06:04	16:37:30–16:07:30	...	0.264	0.479	0.132
	16:54:04–16:30:05	17:07:30–16:37:30	...	0.389	0.722	0.409
	17:30:04–17:06:05	17:37:30–17:07:30	0.413	...	0.665	0.082
	17:54:17–17:30:04	18:07:30–17:37:30	0.328	0.116	0.720	0.070
	18:30:04–18:06:04	18:37:30–18:07:30	...	0.444	0.600	0.195
Sep 14	08:30:04–08:06:04	08:37:30–08:07:30	0.490	...	0.567	0.173
	08:54:04–08:30:04	09:07:30–08:37:30	0.057	0.188	0.591	0.064
	09:30:04–09:06:04	09:37:30–09:07:30	0.539	0.532	0.601	0.022

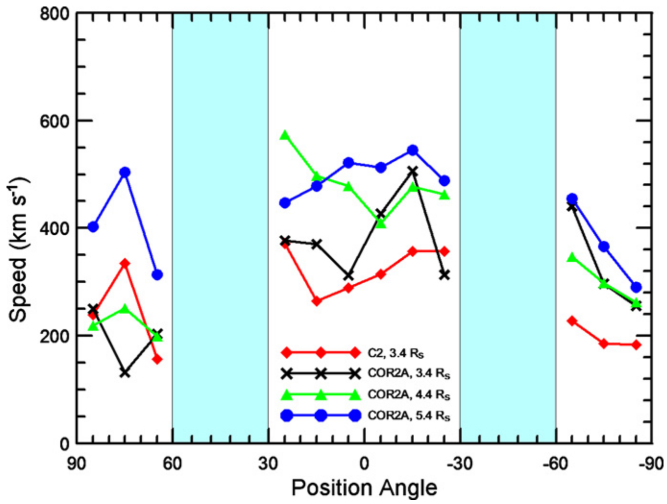

Figure 6. Measurement of the average speed observed in the coronal region vs. solar P.A. (east to solar west over the solar north pole) from a total of 14 C2 and COR2A speed maps on 2007 September 14. The averages are from the different elongations from the Sun in R_s. Shaded regions are locations with few data points as shown in Figure 2.

(A color version of this figure is available in the online journal.)

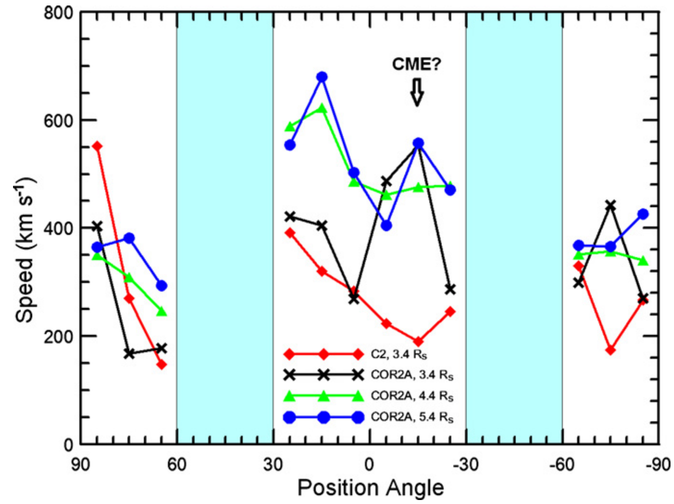

Figure 7. Measurement of the average speed from 21 image pairs from C2 and COR2A observed in the polar coronal region vs. solar P.A. on 2007 September 10.

(A color version of this figure is available in the online journal.)

this result, six C2 speed maps (from 07:52 UT to 09:54 UT) and eight COR2A speed maps (from 07:37 UT to 11:37 UT) over a 4 hr period on 2007 September 14 were averaged for every 10° and 1.0 R_s interval. Each image set was inspected to ensure that no CME was present. The high-speed extent of the polar solar wind can be observed from the east to the west of the Sun over the north polar hole, as in observations from the *Ulysses* spacecraft at this time. We clearly see the change in speed with P.A. from the equatorial regions and across the solar poles and with height from 3.0 R_s upward. The equatorial speeds average somewhat higher at larger distances from the Sun, but all speeds increase over the solar poles to a maximum of around 600 km s^{-1}. C2 and COR2A yield essentially the same results where the images overlap. Figure 7 shows the results for the north polar region on 2007 September 10 plotted in the same way as Figure 6 obtained from 7 C2 (from 16:06 UT to 18:30 UT) and 14 COR2A (from 15:07 to 22:07 UT) speed maps. These again show speeds that are lower and more variable at the equator than over the pole. Generally, higher speeds are observed at larger solar distances.

The measurement during this time period to the northwest is suspect because a small CME may be present. At the solar surface in *SOHO* EIT images, the coronal hole extends from P.A. 25° in the east to −25° in the west and has about the same extent throughout the whole period from 2007 March through September. In the *Ulysses* north polar passage from 2007 September to 2008 June, the high-speed wind extends to about 45° from the north solar pole (McComas et al. 2008).

We show the change of speed with height in the northern polar hole region by averaging the speed maps from −60° to +60° in P.A. Figures 8(a) and (b) show the C2 and COR2A results for the September 10 and 14 data. These averages combine all of the data points from the P.A.s over the polar regions in Figures 6 and 7, assuming conditions are the same across the coronal hole. A visual inspection of the data values presented in Figure 8 show the speed variation for any one point to be about ±25 km s^{-1}. An average outward acceleration is observed and slowly increases until an average speed of ∼600 km s^{-1} is reached at the outer limits of the COR2A image analyses. Because we believe our current results lose significance beyond 5.4 R_s, we do not show them to larger distances. We find approximately the same results for this north polar hole during several other periods from 2007 March 2 to 4.

4. DISCUSSION

The speed maps shown in Figure 2 have the same characteristics for all the sections of data we have analyzed to date. The

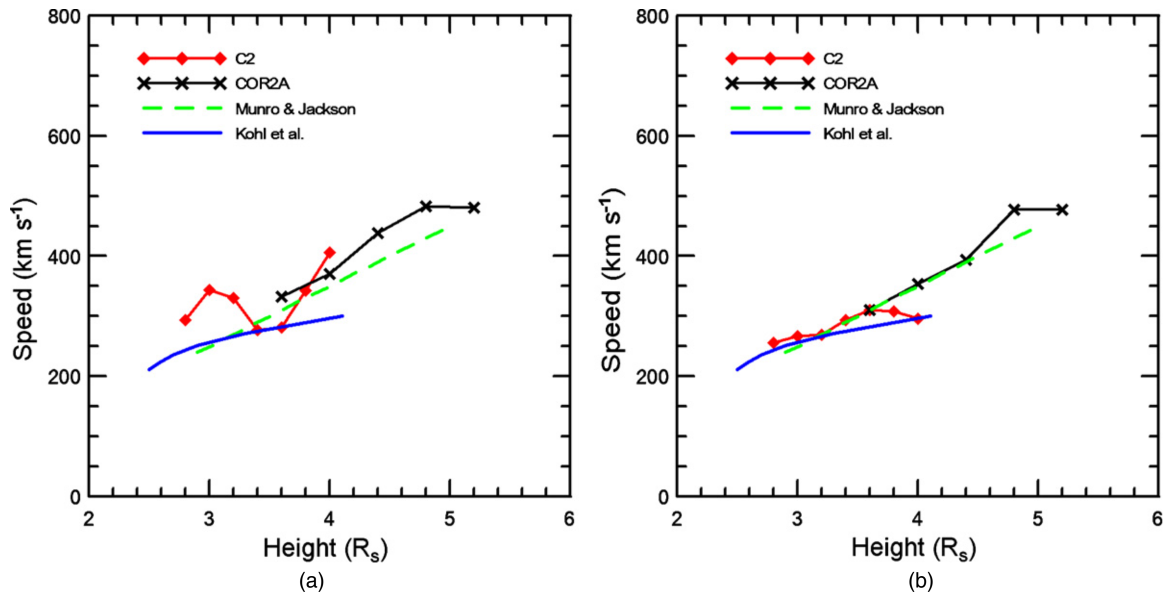

Figure 8. Speed, averaged over P.A.s from −60° to +60°, as a function of height over the solar poles. Additional speed vs. height results from Munro & Jackson (1977) and from Kohl et al. (1998) are superposed. (a) The COR2A coronagraph polar images are averaged from 2007 September 10 at 15:07 to 22:07 UT; C2 images are averaged from nearly the same period. (b) Same as panel (a), but averaged from 2007 September 14 at 07:37 to 11:37 UT.

(A color version of this figure is available in the online journal.)

regions of high speed come and go, and from one speed map to another, specific fast and slow regions can be traced moving outward more or less quickly over time. The characteristic of this motion is akin to long strands of upward-moving and waving seaweed through which fast features propagate at even faster speeds away from the Sun. We provide an animation of this result for a sequence of 14 image pairs of COR2A data in the online journal. The COR2A has the potential to extend this result out to greater distances from the Sun because of the larger heights and higher speeds that can be explored by this instrument. The increased signal to noise with height, determined by the intrinsic image noise and the brightness of coronal structures, will ultimately limit the result.

We have explored parameters in the correlation program that average the data over larger areas, and over different ranges of speed, and find the results are not significantly affected by this. However, for the highest speeds and for data sequences separated by large time intervals, results can become questionable, especially in C2 observations over the poles. Speeds of 800 km s^{-1} imply travel distances of about 1.5 R_s in a 20 minute time interval. Thus, if these speeds or greater exist above 3.5 R_s, it is not possible to measure them in image pairs separated by more than the nominal ∼20 minute cadence. Somewhat greater distances from the Sun in C2 images not directly over the north polar region can be measured since here the edge of the field of view reaches to 6.0 R_s. We know these high speeds exist from a few examples in high-cadence C2 and COR2A observations of a solar jetting response in 2011 (see Yu et al. 2013). These highest speeds would in general not be observable by the cross-correlation technique high in the corona given the 24 minute cadence of these C2 data sequences.

To study the character of the non-uniform flow, as a sample, we present a histogram of the coronagraph data in the north polar region from the locations in common between the C2 and COR2A data in 2007 September 14 (Figure 9). This histogram of just the C2 data shows the distribution by number of the fast- and slow-wind speed regions we observe. The distribution of the fast and slow components shows a decreasing number at higher

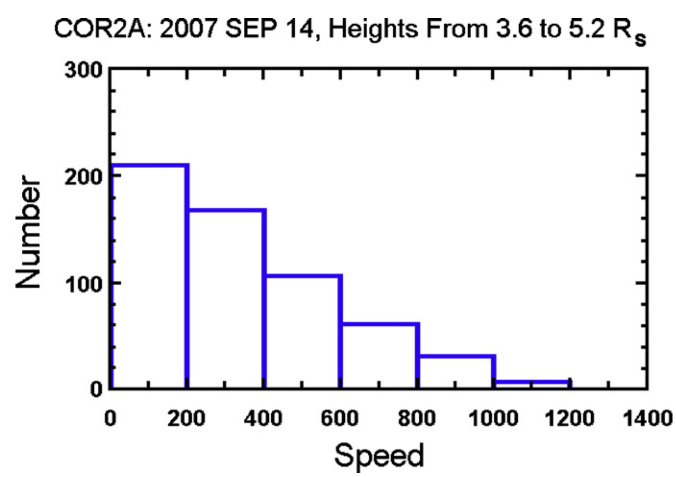

Figure 9. COR2A number histogram of the speeds from the analysis regions between heights 3.6 to 5.2 R_s and from P.A.s −60° to 60° on 2007 September 14.

(A color version of this figure is available in the online journal.)

speeds with no indication here of a bimodal distribution. The two different speeds measured, one fast and one slow, as is suggested by measurements of solar jetting (Cirtain et al. 2007) or by recent Coronal Multi-channel Polarimeter (CoMP) observations, are therefore not present to a significant extent in these observations farther from the Sun. In all of the March 2–4 and September 10 and 14 data sets measured to date, we have found very similar results from both C2 and COR2A observations with no evidence of a bimodal speed distribution.

Averages of the non-static solar wind show that the high-speed regions associated with the coronal hole flow at large distances from the Sun measured in the COR2A images reach a speed of about 600 km s^{-1}. This is about 150 km s^{-1} less than non-varying solar wind in situ observed in polar coronal hole regions seen by *Ulysses* in 2007 (McComas et al. 2008). Taken at face value, this implies that there is still significant acceleration beyond the distances measured by these coronagraphs. To perform a more careful average, it is essential to know the filling factor, or volumetric percentages of the more and the less dense structures. We see a general relationship in this analysis of high speed correlating with higher brightness and thus density (Figure 5 and see Table 1). Thus, using a filling factor that equally weights both the highest and lowest speeds, as we do here, yields an average speed that is somewhat lower than a "true" average speed. A line-of-sight distribution of the many speed results combines data from structures directed away from and toward the observer, and thus this effect provides a true speed over the poles that again should be somewhat higher than our average measured value. These results could vary with solar distance if the filling factor changes with height, as is expected because of the more uniform flow present as observed in *Ulysses* at $\sim$2.0 AU above the solar poles. Because the speed to brightness correlations are significantly less for the COR2A image sets over the image range (see Table 1) than for the C2 images, we suspect as one possibility that analyses from the greater heights in the COR2A image sets lose significance. However, it is additionally possible that the bright and dark regions provide less contrast at large distances from the Sun because the fast regions blend into the background at the highest coronal heights. Although we note that these possibilities exist, an accurate quantization of these effects is beyond the scope of this article.

At lower heights, the regions of slow wind near the solar equator become more variable. This might result from small transient features occurring in or around the streamer belt in the equatorial regions (Sheeley et al. 1997; Wang et al. 1998b) or the inclination and warps in the coronal streamer belt with respect to the solar equator (McComas et al. 1998b, 2000; Phillips et al. 1995). This average speed plot shows another noticeable result over the north polar region. In the solar wind that comes from around the edge of the coronal hole, we find few structures whose outward motion is as well observed elsewhere. This is noticeable as large areas that are blank in Figure 2 between about 30° and 60° P.A. This persists in all of our measurements to date when we limit positive correlations to greater than 0.5 between images. We speculate that this volume between the fast and slow wind may be more chaotic, which would then cause the lower correlations here. At this time, a more thorough exploration of this region lies beyond the scope of this work.

We find that solar wind speed increases with height, and thus its acceleration is observed by averaging our results (Figure 8). The acceleration is observed consistently across all polar coronal hole regions we have analyzed so far. In Munro & Jackson (1977) and subsequent similar polar analyses, the polarization brightness of the average corona is used to determine the large-scale density above large coronal holes. Because the amount of material moving outward above polar coronal holes is relatively unchanging and known (now by direct *Ulysses* measurements), conservation of mass gives the velocity of outward coronal plasma motion, i.e., the average speed of the plasma past any given coronal height above the solar surface where the polarization brightness measurements are made. These analyses also place strict limits on the heating or systematic increase in momentum required to sustain the outward coronal plasma velocity. The Munro & Jackson (1977) result is from the *Skylab* coronagraph observations in 1973; this is a much earlier time period that may not be entirely consistent with the present situation. However, the slightly different mass flux measurements from *Ulysses* during its last solar pass and more recent coronagraph observations (Kohl et al. 1998) show little difference from the earlier Munro & Jackson result (Figure 8). The measurements of polarized brightness used in coronal hole mass flux measurements are necessarily spatial and temporal averages from coronagraph observations and do not indicate the fine structure attributed to plumes and inter-plume regions or any of the fine scale enhancements we see in brightness (and thus density) in these analyses. It is extremely encouraging that the two averages of speed with height above the Sun agree so well.

Near the solar equator, the direct measurement of bright discrete solar wind structures such as jetting enhancements and the results of the correlation program show near identical results, and for these brighter and thus denser structures, we have no doubt that the correlation program measures actual plasma motion. However, we assume that it is possible that the high flow speeds measured in polar coronal areas are not entirely those from outward plasma motion. We note that this possibility is also considered in the analyses of McIntosh (2012) and further explored in recent CoMP observations (McIntosh et al. 2014) much lower in the corona. If the high-speed structures are not entirely plasma flow and if the high speeds retain some outward wave propagation motion, we would not be able to reconcile all of the high speeds we measure by plasma flow alone. However, in light of the good agreement between the average flow speed we measure and the speed determined by mass flux considerations from the coronal polarized brightness data, this effect must be small at the coronal distances we explore here.

5. CONCLUSION

LASCO C2 and *STEREO* COR2A coronagraph images, when analyzed using correlation tracking techniques, show a surprising result in regions above polar coronal holes ordinarily thought of as quiet solar wind. The observed solar wind motion is not a static well-ordered flow with a gradual acceleration, as is normally expected of quiescent polar hole regions. The coronagraph images show outflow above polar coronal holes as having an intermittent and highly variable solar wind speed. It is possible to watch these different-speed patches move outward with solar distances over time. When we compare measurements of this highly variable solar wind using both the C2 and COR2A data sets, we find we can measure essentially the same fast and slow coronal patches of material in both instruments when these are viewing near one another in solar longitude. Measurement of the mean speeds over P.A. are consistent with slow speeds emanating from coronal regions near the solar equator in 2007 and higher speeds associated with polar coronal hole regions. Average speeds derived with height show an acceleration of the high-speed solar wind and are consistent with measurements of mass flux analyses obtained in polar coronal hole regions by Munro & Jackson (1977) and those given by Kohl et al. (1998). These speeds appear slower with less early acceleration than polar coronal hole solar wind speed measurements from the *SOHO* UltraViolet Coronagraph Spectrometer (Kohl et al. 1995) measurements of ionized oxygen (also presented by Kohl et al. 1998).

B.V.J., H.-S.Y., A.B., and P.P.H. were supported at UCSD by NSF grant AGS-1053766, NASA grant NNX11AB50G, and AFOSR grant FA9550–11–1–0324. We are grateful to the LASCO coronagraph group for providing the LASCO C2 images for our use in these analyses and the *STEREO* SECCHI group for providing COR2 images.

REFERENCES

Borovsky, J. E. 2008, JGR, 113, 08110
Borovsky, J. E. 2012, JGR, 117, 6224
Brueckner, G. E., Howard, R. A., Koomen, M. J., et al. 1995, SoPh, 162, 357
Buffington, A., Bisi, M. M., Clover, J. M., et al. 2008, ApJ, 677, 798
Cirtain, J. W., Golub, L., Lundquist, L., et al. 2007, Sci, 318, 1580
Clover, J. M., Jackson, B. V., Buffington, A., Hick, P. P., & Bisi, M. M. 2010, ApJ, 713, 394
Delaboudinière, J.-P., Artzner, G. E., Brunaud, J., et al. 1995, SoPh, 162, 291
Feldman, W. C., Habbal, S. R., Hoogeveen, G., & Wang, Y.-M. 1997, JGR, 102, 26905
Golub, L., Deluca, E., Austin, G., et al. 2007, SoPh, 243, 63
Horn, B. K. P., & Schunck, B. G. 1981, Artif. Intell., 17, 185
Howard, R. A., Moses, J. D., Vourlidas, A., et al. 2008, SSRv, 136, 67
Jackson, B. V., Buffington, A., Clover, J. M., et al. 2013, in AIP Conf. Proc. 1539, Solar Wind Thirteen, ed. G. P. Zank, J. Borovsky, R. Bruno et al. (Melville, NY: AIP), 364
Jackson, B. V., & Hick, P. 1997a, EOS, 78, F537
Jackson, B. V., & Hick, P. P. 1997b, in IAU 23 (Kyoto, Japan), IAU Abstract Book
Jackson, B. V., Hick, P. P., Howard, R., & Dere, K. 1998, EOS, 78, F537
Kohl, J. L., Esser, R., Gardner, L. D., et al. 1995, SoPh, 162, 313
Kohl, J. L., Noci, G., Antonucci, E., et al. 1998, ApJL, 501, L127
McComas, D. J., Bame, S. J., Barker, P., et al. 1998a, SSRv, 86, 563
McComas, D. J., Bame, S. J., Barraclough, B. L., et al. 1998b, GeoRL, 25, 1
McComas, D. J., Barraclough, B. L., Funsten, H. O., et al. 2000, JGR, 105, 10419
McComas, D. J., Ebert, R. W., Elliott, H. A., et al. 2008, GeoRL, 35, 18103
McIntosh, S. W. 2012, SSRv, 172, 69
McIntosh, S. W., Bethge, C., Threlfall, J., et al. 2014, SSRv, submitted
Munro, R. H., & Jackson, B. V. 1977, ApJ, 213, 874
Phillips, J. L., Balogh, A., Bame, S. J., et al. 1994, GeoRL, 21, 1105
Phillips, J. L., Bame, S. J., Barnes, A., et al. 1995, GeoRL, 22, 3301
Sheeley, N. R., Jr., Wang, Y.-M., Hawley, S. H., et al. 1997, ApJ, 484, 472
Shibata, K. 1982, SoPh, 81, 9
Wang, Y.-M., Sheeley, N. R., Jr., Socker, D. G., et al. 1998a, ApJ, 508, 899
Wang, Y.-M., Sheeley, N. R., Jr., Walters, J. H., et al. 1998b, ApJL, 498, L165
Yu, H.-S., Jackson, B. V., Buffington, A., et al. 2014, ApJ, 784, 166
Yu, H.-S., Jackson, B. V., Clover, J. M., & Buffington, A. 2013, in AIP Conf. Proc. 1539, Solar Wind Thirteen, ed. G. P. Zank, J. Borovsky, R. Bruno et al. (Melville, NY: AIP), 90